



Quintuple Plasmonic Fano Resonances for the Sensing Application of Glucose Concentration and Water-soluble Vitamins

Yuchang Li¹ · Jin Huang² · Fang Chen¹

Received: 27 April 2023 / Accepted: 23 May 2023 / Published online: 8 June 2023
© The Author(s), under exclusive licence to Springer Science+Business Media, LLC, part of Springer Nature 2023

Abstract

The quintuple Fano resonance (FR) via a metal–insulator-metal (MIM) waveguide system is presented in this paper, the composite structure is composed of a connected-ring resonator (CRR) and a defective-ring resonator (DRR) coupled to a MIM bus waveguide. Finite difference-time domain method (FDTD) is used to study the transmission characteristics and magnetic field distributions. Results show that the Fano line shapes can be independently tuned by the geometrical parameters, FR1 and FR4 can be tuned by the radius and angle of DRR, while FR2, FR3, and FR5 can be tuned by the radius of CRR and the width of the air path. The calculated maximum refractive index (RI) and glucose solution concentration sensitivities are $1085 \text{ nm}/\text{RIU}$ and $0.136 \text{ nm} \cdot L/g$ (RIU is the refractive index unit), respectively. The maximum optical delay time is about -0.185 ps and 0.08 ps . Also, the proposed device shows a high degree of tolerance. Besides, the proposed sensor can be used to identify water-soluble vitamins B1, B5, and B6. The results of the paper indicate the proposed plasmonic structure may have applications in slow light devices, nano-biosensing, and refractive index sensors.

Keywords Surface plasmon polariton · Metal–insulator-metal · Fano resonance · Refractive index sensor

Introduction

Surface plasmon polariton (SPP), the electromagnetic waves trapped on dielectric-metal interfaces, has attracted much research attention due to its unique properties of overcoming the traditional diffraction limit [1–6]. In the past few decades, SPPs supported by metal–insulator-metal waveguide (MIMW) have been proposed and investigated widely, a large number of MIMW structures with various resonant resonators have been investigated numerically and theoretically [7–12]. For example, Fan et al. studied Fano resonance in MIM waveguide coupled with a Taiji resonator, and a maximal sensitivity of $0.245 \text{ nm} \cdot L/g$ is achieved for glucose solution sensing [13]. A vertically racetrack-ring resonator

was introduced in MIM waveguide by Volkov et al. [14]. A plasmonic Fano resonance filter with FWHM (full width at half maximum) only 5 nm [15].

Fano resonance, initially realized in an atomic system, was first proposed by Ugo Fano in 1961, has potential application in sensors since its sensitivity to the surrounding environment [16–23]. In the past decade, the independent tunability of Fano resonance has attracted lots of attention since its advantage in plasmonic device design [24–28]. However, it is difficult to develop a multiple Fano resonance with independent tunability. Therefore, there is still a need for developing multiple Fano resonances with a simple structure and independent tunability.

The combination of a connected ring resonator and a defective ring resonator into a MIM waveguide structure has been not investigated before. There is no report on the connected ring resonator and defective ring resonator coupling with MIM waveguide for quintuple Fano resonances, which has great potential for multi-channel plasmonic sensing. In this paper, a novel structure has been proposed to design a RI sensor and glucose solution concentration sensor. The structure is composed of a DRR, a CRR, and a middle-air rectangular resonator. The quintuple Fano resonances are attributed to the interference between the bright modes

✉ Fang Chen
chenfang@yangtzeu.edu.cn

Jin Huang
1446942278@qq.com

¹ Institute of Quantum Optics and Information Photonics,
School of Physics and Optoelectronic Engineering, Yangtze
University, Jingzhou 434023, People's Republic of China

² Third People's Hospital, Hubei, Jingzhou 434000,
People's Republic of China

(supported by DRR and CRR) and the dark modes (supported by the middle air rectangular resonator). The position of the FR peaks can be tuned independently by changing different geometrical parameters. The designed quintuple Fano resonance can work as an excellent sensor, a refractive index sensitivity of about $1085 \text{ nm}/\text{RIU}$ and a glucose solution sensitivity of about $0.136 \text{ nm} \cdot L/g$ are obtained. The results of this paper may have potential applications in on-chip plasmonic nanosensors and slow light [29–36].

Geometry and Simulation Method

The proposed quintuple Fano resonance is schematically depicted in Fig. 1, which consists of a MIM waveguide coupled with a CRR (a central air path is located in the middle to connect the ring resonator), a DRR is located on the other side of the MIM waveguide. The grey and white parts in Fig. 1 represent Ag and air, respectively. Silver is used as metal material in the structure and its refractive index can be calculated by the Drude model [37, 38]:

$$\epsilon_m(\omega) = \epsilon_\infty - \frac{\omega_p^2}{\omega^2 + i\omega\gamma_p} \quad (1)$$

The parameters in the model are $\epsilon_\infty = 3.7$, $\omega_p = 9.1 \text{ eV}$, and $\gamma_p = 0.018 \text{ eV}$. Two power monitors are put in the input

and output ports of the bus waveguide, the power can be calculated by:

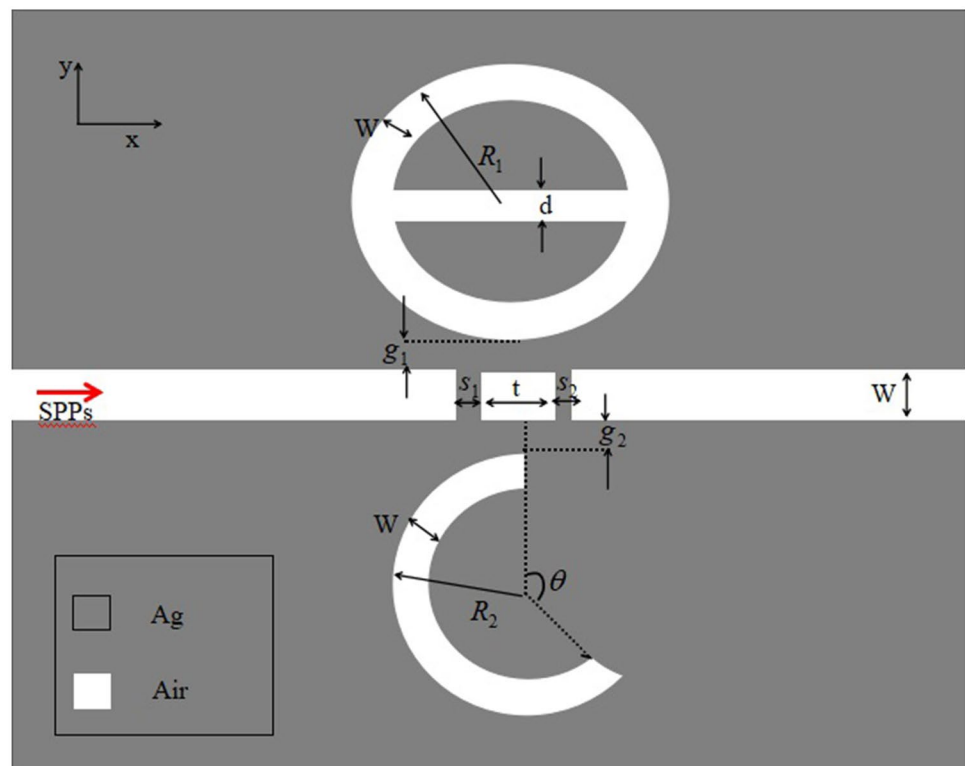
$$P = \frac{\int \text{Re}(E \times H^*) \cdot dS}{2} \quad (2)$$

Then the transmission of the structure can be defined as [39]:

$$T = \frac{P_{\text{out}}}{P_{\text{in}}} \quad (3)$$

The geometric centers of the CRR, the DRR, and the bus waveguide are on the same line. The geometrical parameters are as follows: The width of the central air path is d , the length of the middle air rectangular resonator is t , the coupling distance between the middle air rectangular resonator and the bus waveguide is s_1 and s_2 . The outer radius of CRR and DRR is set as R_1 and R_2 , the notch of the DRR is set as θ , and the coupling distance between the CRR, DRR, and the bus waveguide is g_1 and g_2 . The width of the bus waveguide, CRR and DRR is $w = 50 \text{ nm}$. We use 2D simulation instead of 3D for saving computation time and memory, for actual 3D structure in laboratory, this assumption is acceptable for the thickness larger than $1 \mu\text{m}$. The grid sizes in the FDTD solution are set to be $3 \text{ nm} \times 3 \text{ nm}$, $\Delta t = \frac{\Delta x}{2c}$, where c is the free space speed of light. The simulation area is $1800 \text{ nm} \times 1200 \text{ nm}$, and the distance between the two power monitors is 1250 nm . The calculated size in the coupling region is $2 \text{ nm} \times 2 \text{ nm}$. Perfectly matched layers (PMLs) are applied in the X direction

Fig. 1 The schematic diagram of the proposed multiple Fano resonance plasmonic system composed of a (CRR) and a (DRR)



and metal boundary condition was selected in the Y direction. The proposed MIM waveguide with the middle air rectangular resonator can be made by physical vapor deposition and focused ion beam method. And the CRR and DRR resonators can be made by beam lithography process [40–43].

Based on the standing wave theory, for the DRR, the TM_0 model of the MIM waveguide and the resonance wavelength can be determined by the equations [44]:

$$\tan(kw) = \frac{-2k\epsilon_n\alpha}{\epsilon_m(k^2 + \epsilon_n^2/\epsilon_m^2 + \alpha^2)} \tag{4}$$

$$\alpha = \sqrt{k_0^2(\epsilon_n - \epsilon_m) + k^2} \tag{5}$$

$$\lambda = \frac{2\text{Re}(n_{\text{eff}})L_{\text{eff}}}{n - \varphi/2\pi}, n = 1, 2, 3... \tag{6}$$

where k and k_0 are the wave vector in the waveguide and in the free space. φ is the phase shift induced by the reflection, $\text{Re}(n_{\text{eff}})$ is the real part of the effective refractive index, and n is the order of the resonance mode. n_{eff} can be described as:

$$n_{\text{eff}}(\omega) = \sqrt{\epsilon_{\text{Ag}}(\omega) + \left(\frac{k}{k_0}\right)^2} \tag{7}$$

where the wave vector in the MIM waveguide can be calculated by:

$$k = \sqrt{\beta^2 - \epsilon_{\text{Ag}}(\omega)k_0^2} \tag{8}$$

$k_0 = 2\pi/\lambda$ and β is the wave vector in the free space and the propagation constant. L_{eff} is the effective length of the DRR which can be determined by:

$$L_{\text{eff}} = 2\pi R \frac{360 - \theta}{360} \tag{9}$$

R is the effective radius of the DRR which can be calculated by:

$$R = \frac{R_2 + R_2 - 50}{2} = R_2 - 25 \tag{10}$$

In the proposed plasmonic MIM resonator system, the CRR can be seen as a Fabry–Perot cavity. The resonance wavelength is determined by the equation [45]:

$$\lambda' = \frac{2\text{Re}(n_{\text{eff}})L'_{\text{eff}}}{m - \varphi'/2\pi}, m = 1, 2, 3... \tag{11}$$

According to Eqs. (6) and (11), the resonant wavelength redshifts when L_{eff} increases. Therefore, the effective length of the DRR and CRR can be adjusted to tune the resonant wavelength.

To analyze the Fano resonance mechanism of the proposed structure, the Multimode interference coupled-mode theory (MICMT) is used to calculate the transmission spectrum. The time evolution amplitude a_n of the CRR and DRR resonators can be described as follows [46]:

$$\frac{da_n}{dt} = \left(-j\omega_n - \frac{1}{\tau_{n0}} - \frac{1}{\tau_{n1}} - \frac{1}{\tau_{n2}}\right)a_n + k_{n1}S_{n,1+} + k_{n2}S_{n,2+} \tag{12}$$

$$S_{1-} = -S_{1+} + \sum_n k_{n1}^* a_n \tag{13}$$

$$S_{2-} = -S_{2+} + \sum_n k_{n2}^* a_n \tag{14}$$

$$S_{n,1+} = e^{j\phi_{n1}} S_{1,+} \tag{15}$$

$$S_{n,2+} = e^{j\phi_{n2}} S_{2,+} \tag{16}$$

where ω_n are the resonant frequency of the n_{th} resonant mode, $\tau_{n,i}$ ($i = 1, 2$) are the decay time of the coupling between the resonant cavity and the input and output waveguide, $k_{n,i}$ ($i = 1, 2$) are the coupling coefficient of the n_{th} mode, $\varphi_{n,i}$ are the phase change from input to output part of the n_{th} resonant mode.

When the proposed structure is symmetrically distributed, $\tau_{n1} = \tau_{n2} = \tau_n$ and $\phi_n = \phi_{n1} + \varphi_n$, according to MICMT formula, when $S_{2+} = 0$, the transmission coefficient is obtained as follows:

$$T = \left| \frac{S_{2-}}{S_{1+}} \right|^2 = \left| \sum_n \frac{2e^{j\phi_n}}{-j(\omega - \omega_n)\tau_n + 2 + \frac{\tau_n}{\tau_{n0}}} \right|^2 \tag{17}$$

Figure 2 shows the transmission spectra of the coupled plasmonic system calculated by FDTD. It can be noticed that quintuple Fano resonances (labeled by FR1, FR2, FR3, FR4, FR5) at the resonant wavelength of $\lambda_1 = 696 \text{ nm}$, $\lambda_2 = 830 \text{ nm}$, $\lambda_3 = 952 \text{ nm}$, $\lambda_4 = 1019 \text{ nm}$, $\lambda_5 = 1178 \text{ nm}$. The transmittances of the Fano resonance peaks are 0.41, 0.42, 0.12, 0.24, 0.48, respectively. For further investigation, we can define the asymmetry degree factor p of the Fano line shape as:

$$p = (\lambda_{\text{peak}} - \lambda_{\text{left dip}})/(\lambda_{\text{right dip}} - \lambda_{\text{peak}}) \tag{18}$$

Finally, the asymmetry degree factor p of the five Fano resonances were obtained:

$$p_{FR1} = \frac{696 - 653}{702 - 696} = 7.16 \tag{19}$$

$$p_{FR2} = \frac{831 - 784}{842 - 831} = 4.27 \tag{20}$$

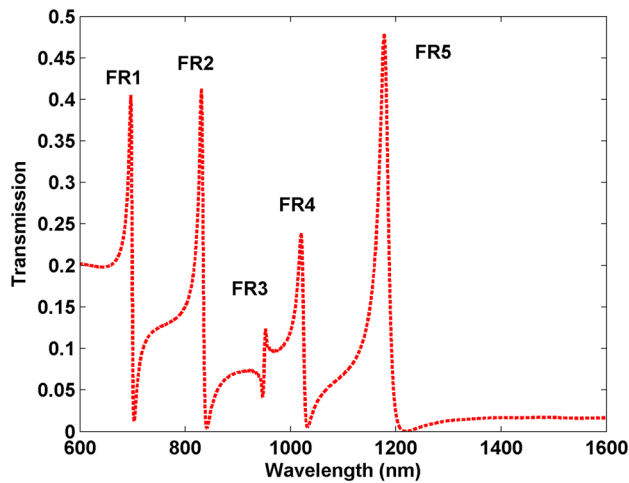


Fig. 2 The transmission spectra of the coupled plasmonic system calculated by FDTD. (The geometrical parameters were set as $w = 50 \text{ nm}$, $s_1 = s_2 = 5 \text{ nm}$, $R_1 = 160 \text{ nm}$, $R_2 = 170 \text{ nm}$ and $t = 60 \text{ nm}$, $g_1 = g_2 = 10 \text{ nm}$, $\theta = 90^\circ$, $d = 50 \text{ nm}$)

$$p_{FR3} = \frac{953 - 847}{965 - 853} = 0.5 \quad (21)$$

$$p_{FR4} = \frac{1020 - 975}{1034 - 1020} = 3.21 \quad (22)$$

$$p_{FR5} = \frac{1178 - 1034}{1218 - 1178} = 3.60 \quad (23)$$

here, $p = 1$ means a symmetric line shape, therefore, the asymmetry degree factor of FR1 is the best. To investigate the mechanism of the Fano resonance, we examined the magnetic-field patterns. Figure 3a and d show the field intensity distribution at resonant wavelength 696 nm (FR1 peak) and 1019 nm (FR4 peak), it can be noticed that almost all the magnetic-field confined in the DRR, indicating that FR1 and FR4 are caused by the interference of the narrow discrete state (DRR resonant mode) and the broad continuum state (middle air rectangular resonator). According to Eq. (2), the orders of resonance mode of FR 1 and FR 4 are 3 and 2 respectively. Figure 3b, c, and e show the field intensity distribution at resonant wavelengths 830 nm (FR2 peak), 952 nm (FR 3 peak), and 1178 nm (FR 5 peak), one can see that almost all the magnetic-field confined in the CRR, indicating that FR2, FR3, and FR5 are caused by the interference of the narrow discrete state (CRR resonant mode) and the broad continuum state (middle air rectangular resonator). The gap plasmonic resonance and cavity plasmonic resonance in CRR offers more flexible control than a popular ring resonator. As can be seen from Fig. 3b, the central air path in the CRR plays an important role in providing more resonance modes since dipolar or quadrupole effects can be induced. Figure 3f shows the incident light is at off-resonance mode 1400 nm, the input SPPs can hardly oscillate in the CRR

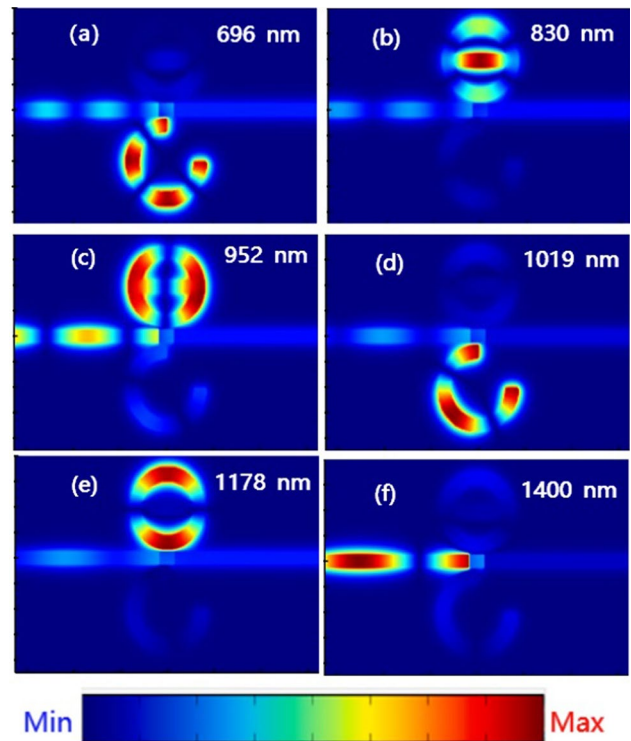


Fig. 3 Magnetic field patterns of **a** FR1 at 696 nm **b** FR2 at 830 nm **c** FR3 952 nm **d** FR4 1019 nm **e** FR5 1178 nm **f** 1400 nm

and DRR, and almost no energy can pass through the output. These above characteristics indicate that FR 1 and FR4 are more sensitive to the dimension of DRR, while FR 2, FR 3, and FR5 are more sensitive to the dimension of CRR.

The influence of the dimensions of the CRR R_1 on the transmittance of the proposed structure is then investigated. As shown in Fig. 4a, when the radius of CRR increases from $R_1 = 140 \text{ nm}$ to 165 nm with a step of 5 nm, it can be seen that the resonant wavelengths of FR2, FR 3 and FR 5 are red-shifted, but the positions of FR 1 and FR 4 keep unchanged. Figure 4b shows the linear relationships between the radius of CRR and the resonant wavelength of FR1, FR 2, FR3, FR4, and FR5. As the radius of CRR increases, FR 2 makes a red-shift from 740 to 860 nm, FR 3 and FR 5 make a red-shift from 845 to 990 nm and from 1049 to 1220 nm, respectively. The transmittance spectra with different air path widths d are shown in Fig. 5a, it can be seen that when the width of the air path increases from $d = 40 \text{ nm}$ to 90 nm with a step of 10 nm, it can be noticed that the resonant wavelengths of FR2, FR 3, FR 5 are red-shifted, but the positions of FR 1, FR 4 keep fixed. Figure 5b shows the linear relationships between the width of the air path and the resonant wavelength of FR1, FR 2, FR3, FR 4, and FR5. As the width of the air path increases, FR 2 makes a blue shift from 849 to 786 nm, FR 3 and FR 5 make a blue shift from 986 to 844 nm and from

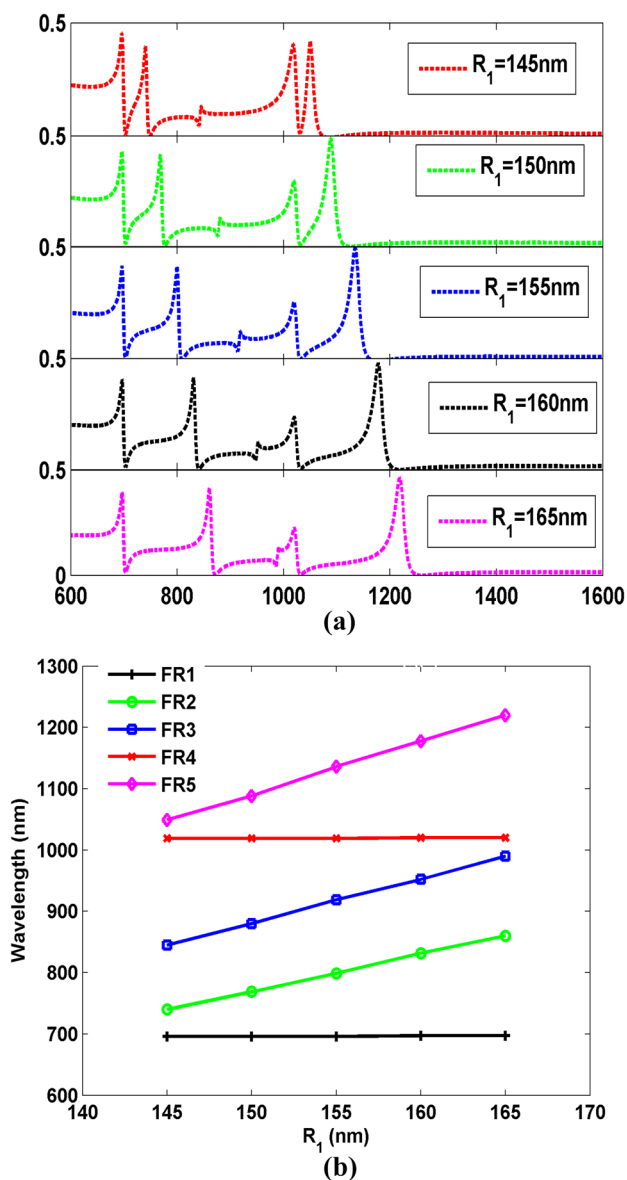


Fig. 4 a The transmission spectra of the plasmonic Fano system with different R_1 b Relationships between the radius of the CRR and the resonance wavelengths

1191 to 1104 nm, respectively. Therefore, the results indicate that FR 2, FR3, and FR5 can be tuned by the radius of the CRR and the width of the air path.

The effect of the dimensions of the DRR R_2 on the transmittance of the proposed structure is studied in detail. As shown in Fig. 6a, when the radius of DRR increases from $R_2 = 165\text{ nm}$ to 185 nm with a step of 5 nm, it can be seen that the resonant wavelengths of FR1, FR4 are red-shifted, but the positions of FR 2, FR 3 and FR 5 keep fixed. Figure 6b shows the linear relationships between the radius of DRR and the resonant wavelengths. As the radius of DRR increases, FR 1 and FR 4 make a red shift from 673 to 757 nm and from 986 to 1115 nm,

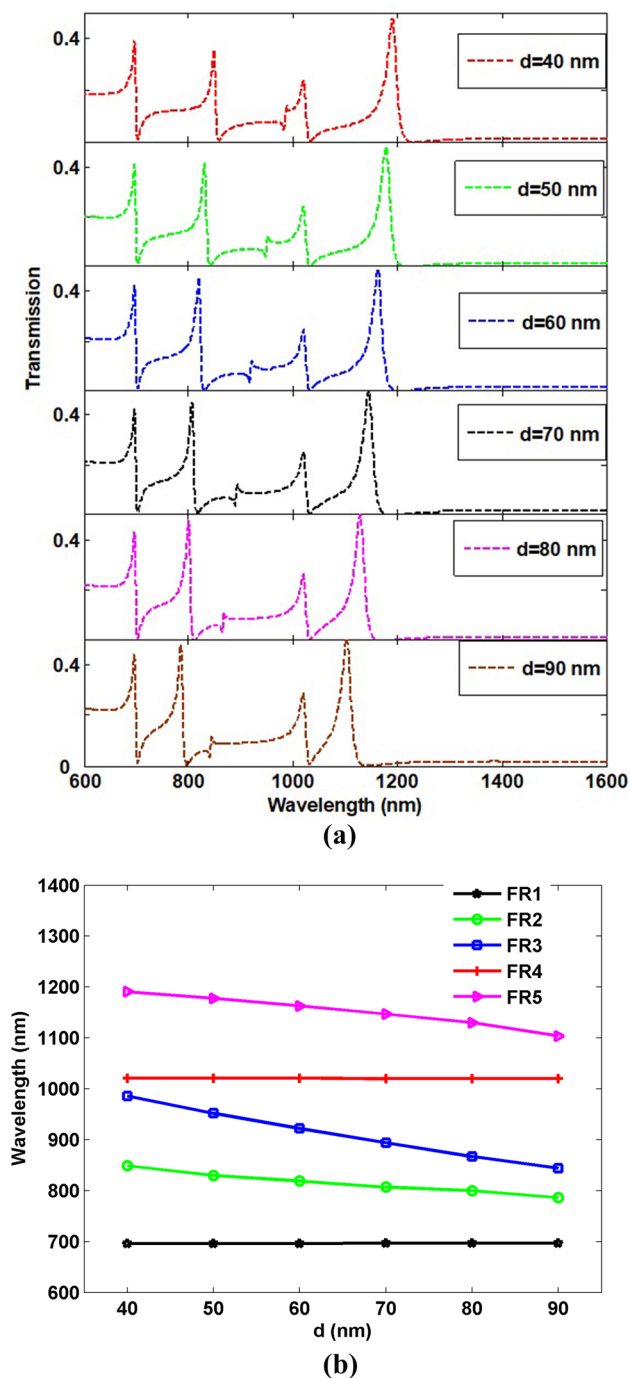
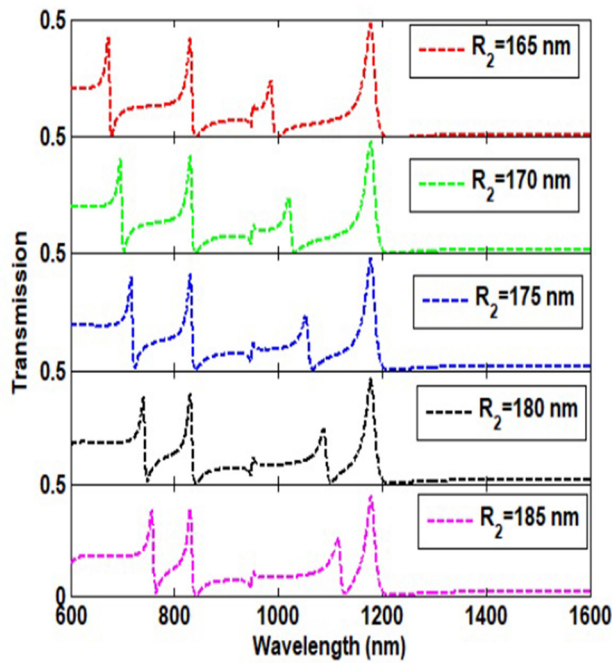
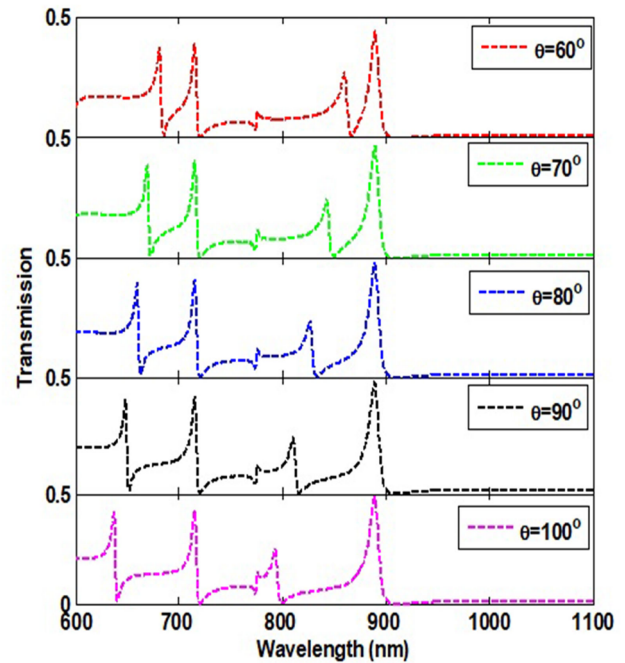


Fig. 5 a The transmission spectra of the plasmonic Fano system with different d b Relationships between the air path width and the resonance wavelengths of FR1 (black), FR2 (green), FR3 (blue), FR4 (red), FR5 (pink)

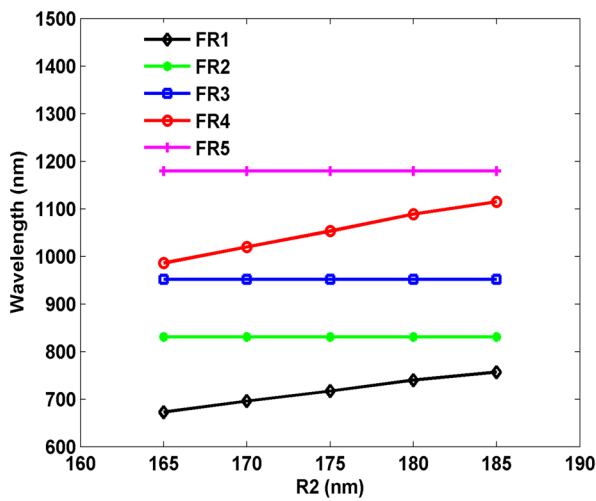
respectively. Figure 7a shows the transmission spectra of the plasmonic Fano system with different notch degrees θ , when the θ increases from $\theta = 60^\circ$ to 100° with a step of 10° , it can be seen that the resonant wavelengths of FR1, FR4 are blue-shifted, but the positions of FR 2, FR 3, and FR 5 keep fixed.



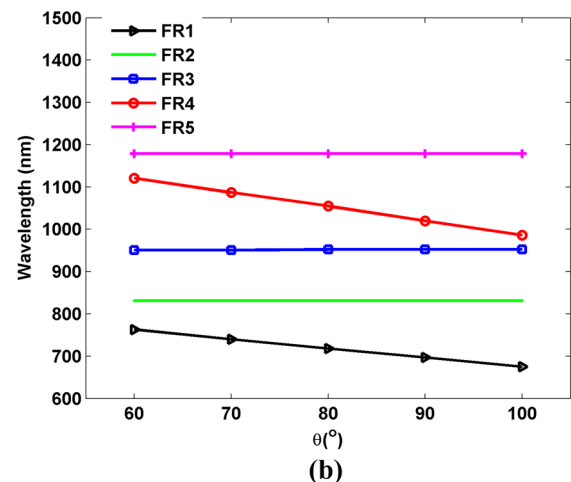
(a)



(a)



(a)



(b)

Fig. 6 **a** The transmission spectra of the plasmonic Fano system with different R_2 **b** Relationships between the radius of the DRR and the resonance wavelengths of FR1 (black), FR2 (green), FR3 (blue), FR4 (red), FR5 (pink)

Figure 7b shows the linear relationships between the notch degree of DRR and the resonant wavelengths. As θ increases, FR 1 and FR 4 makes a blue shift from 763 to 675 nm and from 1121 to 986 nm, respectively. Therefore, the results indicate that FR 1, and FR4 can be tuned by the radius and the notch degree of the DRR.

To gain insight into the sensing application, we investigate the refractive index sensing characteristics of the proposed structure, the refractive index of the medium filled in the CRR and DRR is increased from 1.29 to

Fig. 7 **a** The transmission spectra of the plasmonic Fano system with different θ **b** Relationships between the angle of the defective-resonator and the resonance wavelengths of FR1 (black), FR2 (green), FR3 (blue), FR4 (red), FR5 (pink)

1.37 with a step of 0.02. With $w = 50$ nm, $s_1 = s_2 = 5$ nm, $R_1 = 160$ nm, $R_2 = 170$ nm and $t = 60$ nm, $g_1 = g_2 = 10$ nm, $\theta = 90^\circ$, $d = 90$ nm, the corresponding transmission spectra are shown in Fig. 8a, it can be seen that the resonant wavelength of the quintuple Fano resonances all have a considerable red shift. Figure 8b shows the linear relationships between the refractive index and the resonant wavelengths. The refractive index sensitivity is defined as the shift of the transmittance dip with respect to the change in the refractive index [47]:

$$S = d\lambda/dn(nm/RIU) \tag{24}$$

And the figure of merit (FOM) can be defined as:

$$FOM = \frac{\Delta T}{T\Delta n} \tag{25}$$

The resonant wavelengths of FR to the refractive index were linearly fitted, the relationships are given by:

$$\lambda_{FR1} = 660n + 37.4 \tag{26}$$

$$\lambda_{FR2} = 790n - 11.9 \tag{27}$$

$$\lambda_{FR3} = 850n - 11.9 \tag{28}$$

$$\lambda_{FR4} = 1020n - 6.2 \tag{29}$$

$$\lambda_{FR5} = 1085n + 19.95 \tag{30}$$

Therefore, the sensitivity are approximately 660 nm/RIU, 790 nm/RIU, 850 nm/RIU, 1020 nm/RIU, and 1085 nm/RIU at FR1, FR2, FR3, FR4, and FR5, respectively. The value of maximum FOM reaches 7667.

The proposed plasmonic waveguide structure can be used for biosensing. When the proposed structure is used for glucose concentration sensing, the refractive index of the glucose solution can be calculated by [48]:

$$n = 1.33230545 + 0.00011889C \tag{31}$$

where C is the concentration of glucose solution. As shown in Fig. 9a, when the concentration of glucose solution increases from $C = 0 \text{ g/L}$ to 200 g/L with a step of 50 g/L , it can be seen that the resonant wavelengths of the quintuple Fano resonances all have a considerable red shift. Figure 9b shows the linear relationships between the glucose solution concentration and the resonant wavelengths. The glucose solution sensitivity is defined as the shift of the transmittance dip with respect to the change in the concentration:

$$S = d\lambda/dC(nm \cdot L/g) \tag{32}$$

The resonant wavelengths of FR to the glucose solution concentration were linearly fitted, the relationships are given by:

$$\lambda_{FR1} = 0.07c + 917.8 \tag{33}$$

$$\lambda_{FR2} = 0.086c + 1040 \tag{34}$$

$$\lambda_{FR3} = 0.102c + 1120 \tag{35}$$

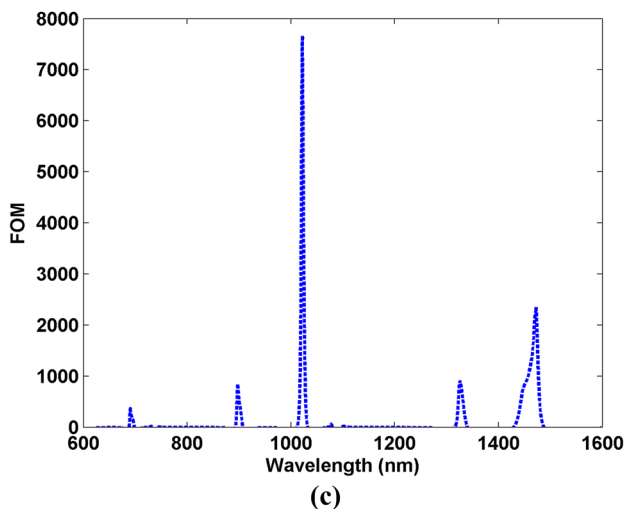
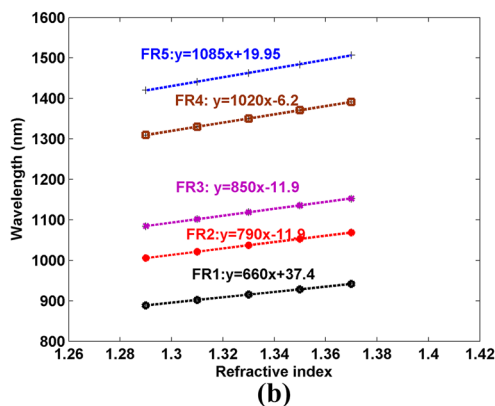
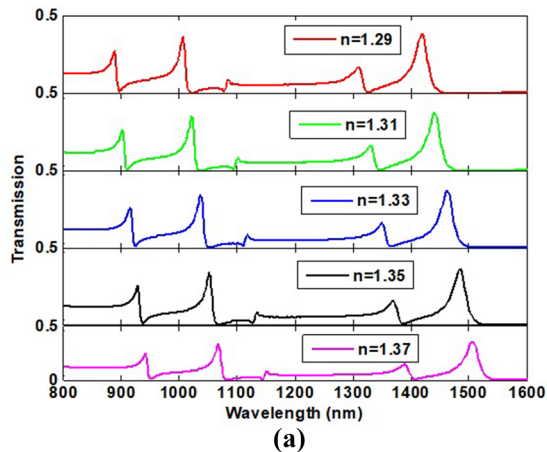


Fig. 8 **a** The transmission spectra of the proposed plasmonic Fano system with different refractive indexes of the CRR and DRR ($\theta = 90^\circ$, $d = 90 \text{ nm}$). **b** Relationships between the refractive index and the resonant wavelengths. **c** FOM of the designed structure

$$\lambda_{FR4} = 0.118c + 1120 \tag{36}$$

$$\lambda_{FR5} = 0.136c + 1465.6 \tag{37}$$

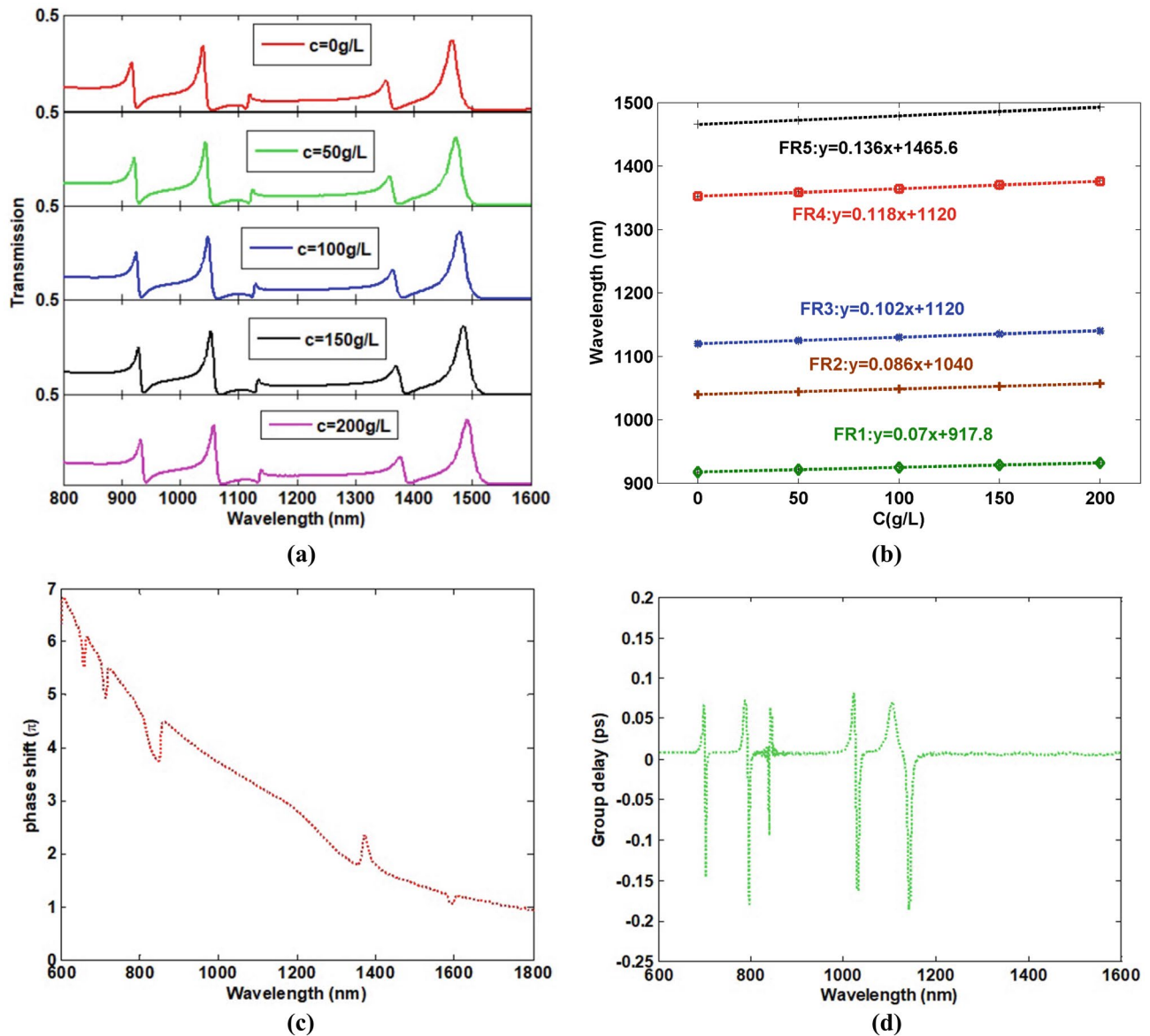


Fig. 9 **a** The transmission spectra of the plasmonic Fano system with different glucose solution concentrations. **b** Relationship between the glucose solution concentrations and the resonance wavelengths. **c** The

phase shift spectrum of the proposed structure. **d** The group delay of the proposed structure

Therefore, the sensitivity are approximately $0.07 \text{ nm} \cdot \text{L/g}$ for FR1, $0.086 \text{ nm} \cdot \text{L/g}$ for FR2, $0.102 \text{ nm} \cdot \text{L/g}$ for FR3, $0.118 \text{ nm} \cdot \text{L/g}$ for FR4, and $0.136 \text{ nm} \cdot \text{L/g}$ for FR5. The sensing performance of other related structures are compared and the results are shown in Table 1. The sensitivity of the present quintuple FR structure is relatively good compared to previous work [49–54]. Another potential application of Fano resonance is slow light. The slow light can be described by the optical delay time $\tau_g(\lambda)$, which can be expressed by [55]:

$$\tau_g(\lambda) = -\frac{\lambda^2}{2\pi c} \frac{d\phi(\lambda)}{d\lambda} \quad (38)$$

$$n_g = \frac{c}{v_g} = \frac{c}{D} \tau_g \quad (39)$$

where, c is the speed of light, $\phi(\lambda)$ is the transmission phase shift, v_g and D are the group velocity and the length of the proposed system. Figure 9c shows the phase shift spectrum of the proposed structure. The group delay of the proposed structure is shown in Fig. 9d, the maximum optical delay time is about 0.08 ps and the maximum negative group delay is about -0.185 ps.

When the proposed structure is used as water-soluble B vitamins concentration sensing, the molecular structures of vitamins can be found from [56–58]. At

Table 1 Comparison of sensing performance to other related plasmonic structures

Structure in other work	Reference	Sensitivity(nm/RIU)
A SRR and DRR resonator with a MIM waveguide	This work	1085
Oblique rectangular cavity	Ref [49]	750
M-type resonator and a baffle with a MIM waveguide	Ref [50]	780
Planar plasmonic structure	Ref [51]	1380
One rectangular and two square nanorod array resonator with a MIM waveguide	Ref [52]	1090
Elliptical cavity resonator	Ref [53]	540
Half ring resonator with MIM waveguide	Ref [54]	753

25 °C, the refractive index of water-soluble B vitamins can be measured by Abbe refractometer, and the average refractive index of water-soluble B vitamins is: $n(\text{Vita min B1}) = 1.3366$, $n(\text{Vita min B5}) = 1.3360$, and $n(\text{Vita min B6}) = 1.3371$. When 1–2 drops of the water-soluble B vitamins dripping into the CRR and DRR resonator. As shown in Fig. 10, FR5 has a larger spectral sensitivity for RI sensing, so FR5 is used to detect water-soluble B vitamins. For FR5, the peak wavelengths of FR5 for B5, B1, and B6 are 1469.1 nm, 1470 nm, and 1470.8 nm, respectively, Recently, an employable detection system can identify wavelength variation as small as 0.1 nm, so the detection of B5, B1, and B6 can be separated from each other. In practice sensing, the device manufacturing accuracy should be considered, from Figs. 4–7, we can see the Fano sensing of the proposed structure is depend on the geometrical sizes, therefore, low manufacturing accuracy will reduce the sensitivity and destroy the linearity. Taking the DRR resonator as an example, Fig. 11 shows the DRR resonator mismatch case. If the DRR resonator rotate by an angle of $\beta = 5^\circ$,

The five Fano resonance peaks attain new sensitivity of 670 nm/RIU, 765 nm/RIU, 820 nm/RIU, 1005 nm/RIU, and 1095 nm/RIU, respectively. For $\beta = -5^\circ$, the sensitivities are about 675 nm/RIU, 780 nm/RIU, 830 nm/RIU, 1005 nm/RIU, and 1100 nm/RIU, respectively. Table 2 show the comparison of sensing performance for DRR resonator rotation mismatch. The result shows the most suitable Fano peak for sensing, FR 5, suffers a minimum and maximum sensitivity increment of 0.92%, and 1.38%, respectively. Compared with the result of work [59], out proposed sensor has a high level of tolerance. Another difficulty in operation is filling the resonator with sensing materials such as glucose concentration and water-soluble vitamins, the non-uniformity filling of the sensing materials will cause a larger sensitivity error. Although the present paper is mainly theoretical simulation, several important experimental work can be found [60, 61].

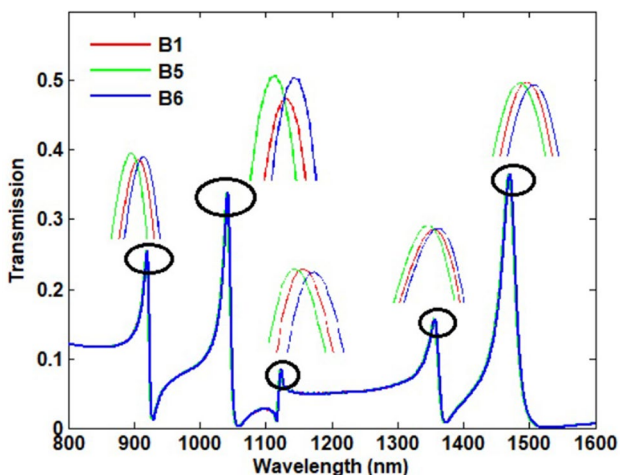


Fig. 10 The transmission spectra of the plasmonic Fano system with different types of water-soluble B vitamins

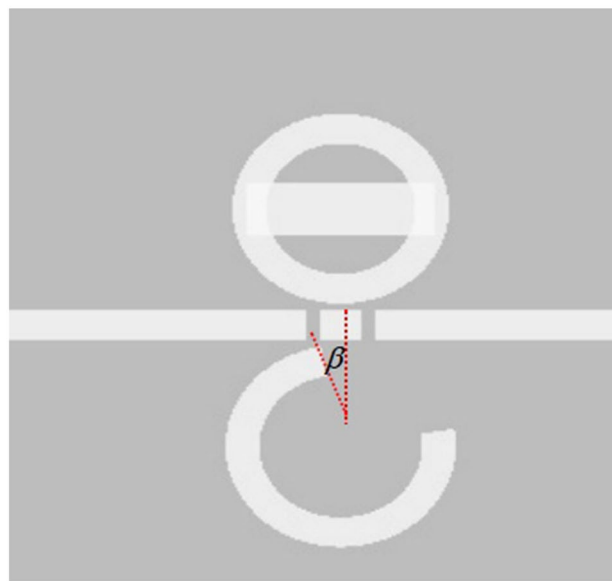


Fig. 11 DRR resonator mismatch by β (in degrees)

Table 2 Comparison of sensing performance for DRR resonator rotation mismatch

DRR rotation β	FR1 (nm/RIU)	FR2 (nm/RIU)	FR3 (nm/RIU)	FR4 (nm/RIU)	FR5 (nm/RIU)
0°	660	790	850	1020	1085
5°	670	765	820	1005	1095
-5°	675	780	830	1005	1100

Conclusion

In conclusion, we present a quintuple Fano resonance based on a DRR, a CRR coupled to a MIM waveguide. Results show that five Fano resonances can be independently tuned by the geometrical parameters, such as the radius of DRR, CRR, the width of the air path, and the notch degree of the DRR. Based on the ultra-sharp Fano line shape, a refractive index sensitivity of about 1085 nm/RIU and a glucose solution sensitivity of about $0.136 \text{ nm} \cdot L/g$ were obtained. And the proposed sensor can be used to identify water-soluble vitamins B1, B5, and B6. The designed quintuple Fano resonance structure can be applied to the areas of on-chip plasmonic nanosensors, and slow light.

Author Contributions Yuchang Li: Conceptualization, Supervision, Investigation, Methodology, Validation, Formal analysis. Jin Huang: Supervision, Writing – review & editing. Fang Chen: Investigation, Methodology, Software, Formal analysis, Writing – original draft, Writing – review & editing. Funding acquisition.

Funding Supported by National Natural Science Foundation of China (Grant No. 11747091). Yangtze Fund for college students' innovation and entrepreneurship. (Grant No. Yz2021280, Yz2022278).

Data Availability Data underlying the results presented in this paper are not publicly available at this time but may be obtained from the authors upon reasonable request.

Declarations

Ethical Approval Not applicable.

Competing Interests The authors declare no competing interests.

References

- Dutta-Gupta D, Martin OJF, Gupta SD, Agarwal GS (2012) Controllable coherent perfect absorption in a composite film. *Opt Express* 20(2):1330–1336
- Genet C, Ebbesen TW (2007) Light in tiny holes. *Nature* 445:39
- Chen F, Yao DZ (2016) Plasmon induced transparency in MIM waveguide side coupled slot resonators system with high sensing sensitivity. *Optik* 127:5115–5119
- Anker JN, Hall WP, Lyandres O, Shah NC, Zhao J, Van Duyne RP (2008) Biosensing with plasmonic nanosensors. *Nat Mater* 7:442–453
- Zhang Q, Huang XG, Lin XS, Tao J, Jin XP (2009) A subwavelength coupler-type MIM optical filter. *Opt Express* 17:7549–7554
- Kim S, Jin J, Kim Y-J, Park I-Y, Kim Y, Kim S-W (2008) High harmonic generation by resonant plasmon field enhancement. *Nature* 453(7196):757–760
- Ebadi SM, Örtégren J, Bayati MS et al (2020) A multipurpose and highly-compact plasmonic filter based on metal-insulator-metal waveguides. *IEEE Photon J* 12(3):4800309
- Bahri H, Hocini A, Bensalah H, Mouetsi S, Ingebrandt S, Pachauri V, Hamani M (2022) A high sensitivity biosensor based on a metal-insulator-metal diamond resonator and application for biochemical and environment detections. *Optik* 271:170083
- Lai W, Wen K, Lin J et al (2018) Plasmonic filter and sensor based on a subwavelength end-coupled hexagonal resonator. *Appl Opt* 57(22):6369–6374
- Salah HB, Bahri H, Hocini A et al (2022) Design of a plasmonic sensor based on a nanosized structure for biochemical application. *Journal of Physics: Conference Series*. IOP Publishing 2240(1):012024
- Pinton N, Grant J, Collins S et al (2018) Exploitation of magnetic dipole resonances in metal-insulator-metal plasmonic nanostructures to selectively filter visible light. *ACS Photonics* 5(4):1250–1261
- Hocini A, Melouki N, Khedrouche D (2021) Design and analysis of near infrared high sensitive metal-insulator-metal plasmonic bio-sensor. *IOP Conference Series: Materials Science and Engineering*. IOP Publishing 1046(1):012003
- Fan HB, Fan HW, Fan HL (2022) Multiple Fano resonance refractive index sensor based on a plasmonic metal-insulator-metal based Taiji resonator. *J Opt Soc Am B* 39:32–39
- Voronin KV, Stebunov YV, Voronov AA, Arsenin AV, Volkov VS (2020) Vertically coupled plasmonic racetrack ring resonator for biosensor applications. *Sensors* 20:203
- Mao JJ, Zhai X, Wang LL et al (2017) Numerical analysis of near-infrared plasmonic filter with high figure of merit based on Fano resonance. *Appl Phys Express* 10(8):082201
- Fano U (1961) effects of configuration interaction on intensities and phase shifts. *Phys Rev* 124:1866–1878
- Chen Z, Gao X, Song X, Wang L, Yu L (2016) side coupled cavity induced Fano resonance and its application in nanosensor. *Plasmonics* 11:307–313
- Ren X, Ren K, Cai Y (2017) Tunable compact nanosensor based on Fano resonance in a plasmonic waveguide system. *Appl Opt* 56:H1–H9
- Zhao W, Leng X, Jiang Y (2015) Fano resonance in all-dielectric binary nanodisk array realizing optical filter with efficient linewidth tuning. *Opt Express* 23:6858–6866
- Chen J, Sun C, Gong Q (2014) Fano resonances in a single defect nanocavity coupled with a plasmonic waveguide. *Opt Lett* 39:52–55
- Wen K, Hu Y, Chen L, Zhou J, He M, Lei L (2017) Tunable multimode plasmonic filter based on side coupled ring groove joint resonator. *Plasmonic* 12:427–431
- Ahmadivand A, Karabiyik M, Pala N (2015) Inducing multiple Fano resonant modes in split concentric nanoring resonator dimers for ultraprecise sensing. *J Opt* 17:085104
- Lee KL, Hsu HY, You ML, Chang CC, Pan MY, Shi X, Ueno K, Misawa H, Wei PK (2017) Highly sensitive aluminum based biosensors using tailorable Fano resonances in capped nanostructures. *Sci Rep* 7:44104
- Hu F, Chen F, Zhang HF, Sun LH, Yu CC (2021) Sensor based on multiple Fano resonances in MIM waveguide resonator system with silver nanorod-defect. *Optik* 229:166237

25. Zhang ZD, Wang HY, Zhang ZY (2013) Fano resonance in a gear shaped nanocavity of the metal-insulator-metal waveguide. *Plasmonic* 8:797–801
26. Wang BH, Wang LL, Li HJ, Zhai X, Xia SX (2016) Two kinds of double Fano resonances induced by an asymmetric MIM waveguide structure. *J Opt* 18:065001
27. Li SL, Wang YL, Jiao RZ, Wang LL, Duan GY, Yu L (2017) Fano resonances based on multimode and degenerate mode interference in plasmonic resonator system. *Opt Express* 25:3525
28. Chen F, Zhang HF, Sun LH, Li JJ, Yu CC (2019) Temperature tunable Fano resonance base on ring resonator side coupled with a MIM waveguide. *Opt Laser Technol* 116:293–299
29. Wu CH, Guo ZC, Chen SX, Yang J, Wen KH (2021) Refractive index sensing based on multiple Fano resonances in a plasmonic defective ring-cavity system. *Res Phys* 27:104508
30. Chao CTC, Chau YFC, Chiang HP (2021) Multiple fano resonance modes in an ultra compact plasmonic waveguide cavity system for sensing applications. *Res Phys* 27:104527
31. Rakhshani MR, Birjandi MAM (2017) High sensitivity plasmonic refractive index sensing and its application for human blood group identification. *Sens Actuators B Chem* 249:168–176
32. Birjandi MAM, Rakhshani MR (2017) Utilizing the metallic nano-rods in hexagonal configuration to enhance sensitivity of the plasmonic racetrack resonator in sensing application. *Plasmonic* 12:999–1006
33. Birjandi MA, Rakhshani MR (2018) A high sensitivity sensor based on three dimensional metal insulator metal racetrack resonator and application for hemoglobin detection. *Photon Nanostruct* 32:28–34
34. Reza RM (2019) Refractive index sensor based on concentric triple racetrack resonators side coupled to metal-insulator-metal waveguide for glucose sensing. *J Opt Soc Am B* 36:2834–2842
35. Chen F, Yao DZ (2016) Realizing of plasmon Fano resonance with a metal nanowall moving along MIM waveguide. *Opt Commun* 369:72–78
36. Zegaar I, Hocini A, Harhouz A et al (2022) Design of a double-mode Plasmonic wavelength filter using a defective circular nanodisk resonator coupled to two MIM waveguides. *Prog Electromagn Res Lett* 104:67–75
37. Zhu J, Li N (2020) MIM waveguide structure consisting of a semicircular resonant cavity coupled with a key-shaped resonant cavity. *Opt Express* 28:19978
38. Johnson PB (1972) Christy RW Optical constants of the noble metal. *Phys Rev B* 6:4370. <https://doi.org/10.1103/PhysRevB.6.4370>
39. Wen K, Hu Y, Chen L, Zhou J, He M, Lei L, Meng Z, Wu Y, Li J (2017) Fano resonance based on end coupled cascaded ring MIM waveguides structure. *Plasmonic* 12:1875–1880
40. Wang Q, Ouyang Z, Lin M, Liu Q (2018) Independently tunable Fano resonances based on the coupled hetero-cavities in a plasmonic MIM system. *Materials* 11:1675
41. Chou Chao CT, Chou Chau YF, Chen SH et al (2021) Ultrahigh sensitivity of a plasmonic pressure sensor with a compact size. *Nanomaterials* 11(11):3147
42. Bensalah H, Hocini A, Bahri H (2022) Design and analysis of a mid-infrared ultra-high sensitive sensor based on metal-insulator-metal structure and its application for temperature and detection of glucose. *Prog Electromagn Res M* 112:81–91
43. Bensalah H, Hocini A, Bahri H et al (2022) A plasmonic refractive index sensor with high sensitivity and its application for temperature and detection of biomolecules. *J Opt* 1–12:00922
44. Li ZF, Wen KH, Chen L, Lei L, Zhou JY (2019) Refractive index sensor based on multiple Fano resonances in a plasmonic MIM structure. *Appl Opt* 58:4878–4883
45. Chen C, Oh SH, Li M (2020) Coupled mode theory for plasmonic resonators integrated with silicon waveguides towards mid-infrared spectroscopic sensing. *Opt Express* 28:36
46. Li SL, Wang YL, Jiao RZ, Wang LL, Duan GY, Yu L (2017) Fano resonances based on multimode and degenerate mode interference in plasmonic resonator system. *Opt Express* 25:3525–3533
47. Chen Y, Xu Y, Cao J (2019) Fano resonance sensing characteristics of MIM waveguide coupled square convex ring resonator with metallic baffle. *Res Phys* 14:102420
48. Xu D, Yan S, Yang X, Su H, Wu X, Hua E (2021) A nanoscale structure based on a ring with metachstick shape cavity for glucose concentration and temperature detection. *IEEE Sens J* 21:4442–4450
49. Pang SF, Huo YP, Xie Y, Hao LM (2016) Fano resonance in MIM waveguide structure with oblique rectangular cavity and its application in sensor. *Opt Commun* 381:409–413
50. Qiao L, Zhang G, Wang Z, Fan G, Yan Y (2019) Study on the Fano resonance of coupling M type cavity based on surface plasmon polaritons. *Opt Commun* 433:144–149
51. Wang JQ, Fan CZ, He JN, Ding P, Liang EJ, Xue QZ (2013) Double Fano resonance due to interplay of electric and magnetic plasmon modes in planar plasmonic structure with high sensing sensitivity. *Opt Express* 21:2236–2244
52. Rakhshani MR (2021) Refractive index sensor based on dual side coupled rectangular resonators and nanorods array for medical applications. *Opt Quantum Electron* 53:232
53. Haffar RE, Farkhsi A, Mahboub O (2020) Optical properties of MIM plasmonic waveguide with an elliptical cavity resonator. *Appl Phys A* 126:486
54. Li X, Zhang Z, Guo F, Huang Y, Zhang B, Zhang L, Yang Q, Tan Y, Liu X, Bai H, Song Y (2019) Tunable plasmonically induced reflection in HRR-coupled MIM waveguide structure. *Optik* 199:163353
55. Lu H, Liu XM, Mao D, Gong YK, Wang GX (2011) Induced transparency in nanoscale plasmonic resonator system. *Opt Lett* 36:3233–3235
56. Biplab R, Ashutosh D, Beauty M, Debadrita R, Kumar MD, Subires B, Nath RM (2020) Study to explore host guest inclusion complexes of vitamin B1 with CD molecules for enhancing stability and innovative application in biological system. *J Mol Liq* 298:0167–7322
57. Davide C, Barbara C, Debora S, Caterina F, Antonello F, Simonetta F, Elisa CM (2021) Molecular properties of bare ad microhydrated vitamin B5 calcium complexes. *Int J Mol Sci* 22:692
58. Takashi K, Takaomi K, Anna O, Michihiro L, Yasushi H et al (2021) Vitamin B6 efficacy in the treatment of nonalcoholic fatty nutrition. *J Clin Biochem Nutr* 68:181–186
59. Hassan MF, Sagor RH, Tathif I et al (2020) An optimized dielectric-metal-dielectric refractive index nanosensor. *IEEE Sens J* 21(2):1461–1469
60. Zhou Z, Tan C, Zheng Y et al (2013) Electrochemical signal response for vitamin B1 using terbium luminescent nanoscale building blocks as optical sensors. *Sens Actuators B Chem* 188:1176–1182
61. Pires AR, Araújo AN, Montenegro MCBSM et al (2008) New ionophores for vitamin B1 and vitamin B6 potentiometric sensors for multivitaminic control. *J Pharm Biomed Anal* 46(4):683–691

Publisher's Note Springer Nature remains neutral with regard to jurisdictional claims in published maps and institutional affiliations.

Springer Nature or its licensor (e.g. a society or other partner) holds exclusive rights to this article under a publishing agreement with the author(s) or other rightsholder(s); author self-archiving of the accepted manuscript version of this article is solely governed by the terms of such publishing agreement and applicable law.